Fine-scale dynamics of calcite precipitation in a large hardwater lake

Nicolas Escoffier [a],[*], Pascal Perolo [a], Gaël Many [a], Natacha Tofield Pasche [b], Marie-Elodie Perga [a]

[a] *Institute of Earth Surface Dynamics, University of Lausanne, Switzerland*
[b] *Limnology Center, ENAC, Ecole Polytechnique Fédérale de Lausanne, Switzerland*

HIGHLIGHTS

- Calcite precipitation is a main yet poorly resolved process of lakes' carbon cycle.
- Calcite precipitation is finely quantified in Lake Geneva using high-frequency data.
- Seasonally, calcite precipitation depends on the duration of lake stratification.
- Daily calcite precipitation scales tightly to the intensity of primary production.
- Generated carbon fluxes are of similar magnitude as net ecosystem production.

GRAPHICAL ABSTRACT
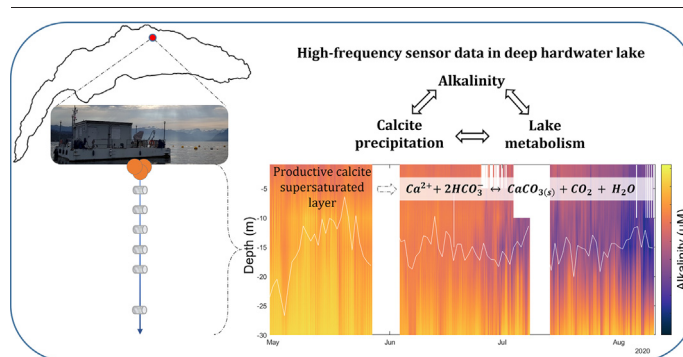
ABSTRACT

In hardwater lakes, calcite precipitation is an important yet poorly understood process in the lacustrine carbon cycle, in which catchment-derived alkalinity (Alk) is both transformed and translocated. While the physico-chemical conditions supporting the supersaturation of water with respect to calcite are theoretically well described, the magnitude and conditions underlying calcite precipitation at fine temporal and spatial scales are poorly constrained. In this study, we used high frequency, depth-resolved (0–30 m) data collected over 18 months (June 2019 – November 2020) in the deeper basin of Lake Geneva to describe the dynamics of calcite precipitation fluxes at a fine temporal resolution (day to season) and to scale them to carbon fixation by primary production. Calcite precipitation occurred during the warm stratified periods when surface water CO_2 concentrations were below atmospheric equilibrium. Seasonally, the extent of Alk loss due to calcite precipitation (i.e., [30–42] $g\,C\,m^{-2}$) depended upon the level of Alk in surface waters. Moreover, interannual variability in seasonal calcite precipitation depended on the duration of stratification, which determined the volume of the water layer susceptible to calcite precipitation. At finer timescales, calcite precipitation was characterized by marked daily variability with dynamics strongly related to that of planktonic autotrophic metabolism. Increasing daily calcite precipitation rates (i.e., maximum values 9 $mmol\,C\,m^{-3}\,d^{-1}$) coincided with increasing net ecosystem production (NEP) during periods of enhanced water column stability. In these conditions, calcite precipitation could remove as much inorganic carbon from the productive layers as NEP. This study provides mechanistic insights into the conditions driving pelagic calcite precipitation, and quantifies its essential contribution to the coupling of organic and inorganic carbon cycling in lakes.

1. Introduction

Inland waters are essential components of the global carbon cycle. Despite their modest contribution to the Earth's surface area, riverine and lacustrine systems act as reactors rather than passive transporters of terrestrial carbon to the ocean. For ~1 Pg C yr^{-1} reaching the ocean, ~

* Corresponding author at: Institute of Earth Surface Dynamics, Geopolis, University of Lausanne, CH-1015 Lausanne, Switzerland.
  E-mail address: nicolas.escoffier@unil.ch (N. Escoffier).

0.5 Pg C yr^{-1} get buried in inland waters while ~1 to 3 Pg C yr^{-1} are returned as CO_2 to the atmosphere (Cole et al., 2007; van Hoek et al., 2021). Due to their longer water residence time, lakes and reservoirs play a crucial role in carbon transformations along the freshwater continuum (Tranvik et al., 2009). Lake metabolism (i.e., the balance between lacustrine photosynthesis and mineralization of terrestrial and autochthonous organic matter) has traditionally been considered the primary process of carbon transformation (Duarte and Prairie, 2005; del Giorgio et al., 1999). This view, however, has been challenged, as studies have revealed that inorganic carbon transformations and carbonate equilibria could override organic carbon processes in hardwater lakes (Finlay et al., 2009; Stets et al., 2009).

Among the inorganic carbon reactions in lakes, calcium carbonate (calcite) precipitation represents a pivotal biogeochemical process transforming alkalinity (Alk) inputs derived from carbonate weathering in the catchment (Müller et al., 2016). In lakes with Alk above ~1 mM (i.e., approximately half of the lakes worldwide; Marcé et al., 2015), calcite precipitation is expected to occur during the warm season. Calcite precipitation acts first as an inorganic carbon sink to the sediments and then as a potential carbonate counter pump restoring dissolved inorganic carbon (DIC) in surface waters (Andersen et al., 2017). Recent estimates suggest that carbon losses due to calcite precipitation equal organic carbon burial in lakes and reservoirs (i.e., 0.03 vs 0.15 Pg C yr^{-1}), hence supporting its relevance for the global lacustrine carbon budget (Khan et al., 2022). However, the current knowledge of the mechanisms of calcite precipitation in lakes and the magnitude of inorganic carbon fluxes is limited, thereby representing a key frontier in the understanding of lakes' carbon cycle.

The physico-chemical conditions supporting calcite supersaturation (e.g., Alk, Ca^{2+} concentrations, water temperature and pH) are well described (Plummer and Busenberg, 1982). However, the conditions underlying the dynamics of calcite precipitation and nucleation, at fine temporal and spatial scales, remain poorly understood. Calcite precipitation in lakes has been related to primary production due to its effect on CO_2 removal and increase of pH, displacing the carbonate equilibria towards calcite supersaturation (Müller et al., 2016; Stabel, 1986). Yet, different mechanisms are suggested regarding the role of photo-autotrophs in the nucleation and precipitation of the mineral. In shallow macrophyte-dominated lakes and littoral areas, calcite precipitation has been described as a controlled process allowing photo-autotrophs to cope with CO_2 limitations by using Alk (i.e. HCO_3^-) while preventing a detrimental pH increase for photosynthesis (Andersen et al., 2019). In these conditions, both calcite supersaturation and precipitation are driven by littoral primary producers, as observed in calcifying marine organisms (Gattuso et al., 1999), for which calcification facilitates resource acquisition in low-light and nutrient-depleted conditions (McConnaughey and Whelan, 1997). In the pelagic domains of deeper lakes, calcite precipitation is regarded as a biologically induced process (Hodell et al., 1998) whereby primary production favors calcite supersaturation without necessarily controlling its precipitation. In most case-studies in oligotrophic systems, calcite precipitation has been associated with picoplankton, especially picocyanobacteria. In contrast to macrophytes, picoplankton would induce a passive calcite nucleation mechanism linked to the alkalinization of their microenvironment during photosynthesis and the specific structure of their cellular membranes (Dittrich et al., 2004; Obst et al., 2009). In other studies, the precipitation of calcite has also been related to micro-heterotrophs and extracellular polymeric substances (Zhu and Dittrich, 2016), or catchment-derived detrital particles (Effler and Peng, 2012), thus, further expanding the range of environmental conditions and drivers supporting pelagic calcite precipitation in lakes.

The tenuous link between calcite precipitation and primary production has been previously explored through their molar ratios (expressed as the ratio of calcite precipitation to NEP, referred to as α in Khan et al., 2021). Such an expression allows considering the effect of calcite precipitation on total DIC removed and explaining deviations from the theoretical 1:1 metabolic relation between DIC and dissolved oxygen (DO) sometimes observed in hardwater systems (Khan et al., 2020). Nonetheless, few estimates

are available, especially for deep lakes, a lack of data due to the methodological approaches used to study calcite precipitation. In most cases, calcite precipitation is assessed from sediment trap and core data (Hodell et al., 1998) or from calcium and Alk mass balance calculations derived from water sampling (Perga et al., 2016) or modelling (Homa and Chapra, 2011). While these approaches enable inferring seasonal precipitation rates, they do not allow for a detailed examination of the process at fine-scale and the delineation of mechanisms. This is an important limitation for refining its environmental drivers at a short to medium time scale and to foresee the effects of global environmental changes on its dynamics in lakes.

Lake Geneva is the largest hardwater lake in western Europe and represents a suitable system to address these questions. Calcite precipitation is an important process in the lake (Müller et al., 2016; Perga et al., 2016), which has been related to distinct features across its basins. In the shallower part of the lake, the authigenic calcite precipitation has been linked to the photosynthetic activity of biofilms or planktonic species (Martignier et al., 2017; Pacton et al., 2012). In the larger basin of the lake, the phenology of the process is, however, more complex owing to a deeper bathymetry, dynamic mixing regimes and the occurrence of allochthonous sedimentary inputs along the authigenic calcite sedimentation (Escoffier et al., 2022; Graham et al., 2016).

In this context, the present study aimed to (*i*) assess the use of high-frequency multi-parameter sensor data to trace the fine-scale dynamics of pelagic calcite precipitation in the deeper basin of Lake Geneva, (*ii*) estimate the magnitude of the process at different time scales (day to season) and infer the importance of calcite precipitation for the lacustrine carbon budget, and (*iii*) investigate the coupling of calcite precipitation with the dynamics of primary production in surface waters of Lake Geneva.

2. Material and methods

2.1. Study site

With a surface area of 580 km^2 and a total volume of 89 km^3, Lake Geneva is the largest hardwater lake in Western Europe (Fig. 1). Lake Geneva has a mean water residence time of 11 years, and defines part of the border between France and Switzerland, at 372 m above sea level. The lake is composed of two distinct basins, the Petit-Lac (maximum depth 70 m) and the Grand-Lac (maximum depth 309 m), which hold 4 % and 96 % of the total water volume, respectively. Lake Geneva is an oligomictic lake - complete mixing of the deep basin happens every seven years on average during exceptionally cold winters (Gaudard et al., 2017). The water column is stratified from April – May to September – October. Stratification favors enhanced internal motions, which are dominated by vertical baroclinic dislocations (Fernández Castro et al., 2021).

The moderately alkaline waters of the lake (ranging between 1.2 and 2 mM) result from the weathering of carbonate rocks in the lake's 7395 km^2 catchment. The Rhône River drains the Alps in the eastern part of the lake and represents the main hydrological input (~ 80 %). The remainder is contributed by tributaries draining the Jura mountains to the north-west and the pre-Alps in the south, while rainfall represents a minor contribution (Halder et al., 2013). The current trophic state of Lake Geneva is oligo-mesotrophic (Perga et al., 2016). Lake water quality has been monitored on a monthly to fortnightly basis since the late 1950s at point SHL2 (Fig. 1; OLA-IS, AnaEE-France, INRAE of Thonon-les-Bains, and CIPEL; Rimet et al., 2020).

2.2. Continuous multi-sensor data

The high-frequency dataset used in this study was acquired from the LéXPLORE platform, which is a 100 m^2 pontoon deployed in 2019 on Lake Geneva (Wüest et al., 2021). The platform is located 570 m from the lake's northern shore (close to the city of Lausanne, Fig. 1) and anchored at a depth of 110 m.
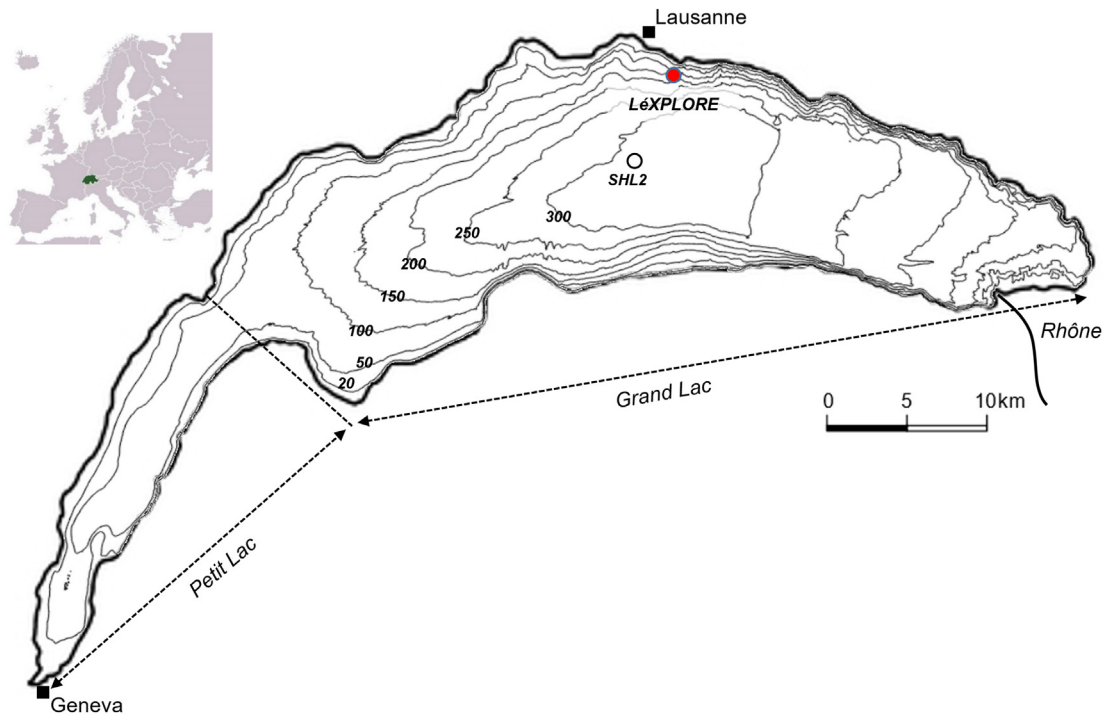
Fig. 1. Lake Geneva and locations of the LéXPLORE scientific platform and SHL2 sampling point.

At the LéXPLORE platform, a sensor line was installed in June 2019 to measure water temperature (T), electrical conductivity and pH every 15 min at 6 depths in the top 30 m surface layer (i.e., 0.5, 5, 10, 15, 20 and 30 m). Temperature and electrical conductivity were measured using Hobo U24–001 Conductivity sensors (Onset, MA, U.S.A.) while pH was measured using Hobo MX2501 sensors (Onset, MA, U.S.A.). The metrology of the sensors was controlled every 4 to 6 weeks during maintenance surveys. Accordingly, sensors were immersed in a common bath in laboratory and their data were compared to that of an independent multi-parameter probe (Multi 3430, Set G, WTW) equipped with SenTix 940 and TetraCon 925 sensors specifically calibrated each time. The in-situ sensor data were post-corrected for drift whenever necessary and possible, assuming linear drift. pH Hobo MX2501 sensors were calibrated with fresh specific buffers before each deployment and verified to be within a consistent $+/- 0.05$ pH unit range.

Air temperature, wind speed and direction, relative humidity, shortwave radiations and atmospheric pressure were recorded at the LéXPLORE platform, 5 m above the lake surface, every 15 min using a Campbell Scientific automatic weather station. For this study, high-frequency data were recorded between June, 4th 2019 and November, 11th 2020. All high frequency data were averaged hourly.

2.3. Discrete sampling and analytical procedures

In parallel with high frequency data, water samples were regularly collected at LéXPLORE at each of the six depths covered by sensor measurements using a Niskin bottle (KC Denmark, Silkeborg, Denmark). Samples for the determination of major ions and total alkalinity (Alk) were filtered immediately on the platform using 0.22 μm pore size polyethersulfone syringe filters (Minisart, Sartorius AG, Goettingen, Germany). Samples were stored at 4 °C in the dark in sterile polypropylene tubes (Greiner Bio-One) for analyses within two weeks. Ion chromatography (MetrOhm, Herisau, Switzerland) was used to measure major anion and cation concentrations, with a detection limit of 0.1 mg L^{-1}. Colorimetric titration using methylorange to a final pH of 3.2 implemented in a SmartChem 200 analyzer (AMS Alliance, France) was used to determine Alk, with a precision of 2 % measured on external prepared standards.

Sediment traps were deployed at 10 m and 30 m depth in 2020 at LéXPLORE. Sediment trap samples were retrieved every four to six weeks and freeze-dried in the laboratory. The total inorganic carbon (TIC) content of the samples was measured using a Soli TOC analyzer (Elementar Gmbh, Germany).

2.4. Data analyses and reduction

To estimate calcite precipitation rates from high frequency sensor data, several steps were followed, as detailed in the next subsections. In brief, (*i*) conductivity data were used to estimate Alk, which, along pH data, allowed us to (*ii*) calculate the other descriptors of the carbonate system (i.e., partial pressure of CO_2 (pCO_2) and DIC as the sum of CO_2, HCO_3^- and CO_3^{2-} concentrations) at high frequency. Then, (*iii*) using the pluri-annual monitoring data of Lake Geneva to constrain the relation between the saturation index of CO_2 (i.e., Ω_{CO2}) and the saturation index of calcite (Ω_{CaCO3}), Ω_{CO2} was calculated from high-frequency data and used as a proxy to resolve the depth of the calcite supersaturated water layer. In the calcite supersaturated layer, calcite precipitation rates were calculated from Alk losses.

2.4.1. Alkalinity timeseries

Specific conductance at 25 °C (C_{25}) was calculated from electrical conductivity and water temperature and related to discrete Alk data by linear regression, following the approach by Groleau et al. (2000). The equation of the significant linear correlation between C_{25} and Alk data was subsequently used to transform C_{25} data into continuous Alk timeseries.

2.4.2. Carbonate system calculations

Timeseries of Alk, pH, T along with measurement depth at LéXPLORE were used to calculate the remaining parameters describing the carbonate system (i.e., pCO_2 and DIC) at each depth and timestep using the CO2SYS function developed for the MATLAB program by van Heuven et al. (2011), and the specific constants from Millero (1979) for freshwaters.

2.4.3. Calcite precipitation rate estimation

In a study of several hardwater lakes in Switzerland, including Lake Geneva, Müller et al. (2016) observed that calcite precipitation occurred when

the lake waters were undersaturated with respect to CO_2 (i.e., when Ω_{CO2}, the ratio of the pCO_2 in water divided by the pCO_2 in atmosphere, was ≤ 1). Accordingly, we used the pluri-annual monitoring data of Lake Geneva to investigate the link between Ω_{CO2} and Ω_{CaCO3} and evaluate the possibility of using Ω_{CO2} as a proxy for calcite saturation conditions, and, hence, potential calcite precipitation.

Pluri-annual pCO_2 data and CO_3^{2-} concentrations in the lake were calculated from Alk, pH, and T data measured at 20 depths (i.e., from the surface down to 309 m) at the long-term monitoring station (SHL2) during the 2012–2016 period, using the CO2SYS function previously described, and Ω_{CO2} was calculated assuming a constant atmospheric pCO_2 of 400 ppm.

The saturation index for calcite was calculated using the open-source chemical equilibrium software Visual Minteq version 3.1., as (Eq. (1)):

$$\Omega_{CaCO3} = \frac{\{Ca^{2+}\}\{CO_3^{2-}\}}{K_{s0}} \tag{1}$$

where $\{Ca^{2+}\}$ and $\{CO_3^{2-}\}$ are the activities of Ca^{2+} and CO_3^{2-} calculated from their respective concentrations at SHL2 using the Debye-Hückel approximation and the ionic strength determined from major ion concentrations, and accounting for possible complexation and neutral species. K_{s0} corresponds to the solubility constant of calcite, which was adjusted to measured temperatures according to Plummer and Busenberg (1982).

The graphical representation of the pluri-annual data of Ω_{CO2} as a function of Ω_{CaCO3} revealed a nonlinear pattern of increasing calcite saturation with decreasing Ω_{CO2} (See supplementary Fig. S1), consistent with former observations (Müller et al., 2016). Using the corresponding nonlinear fit, we retained a Ω_{CO2} value of 0.75 as a conservative threshold below which calcite precipitation is possible. Indeed, below such Ω_{CO2} threshold, values of Ω_{CaCO3} were always ≥ 2.5, which has been shown as a minimum calcite supersaturation level allowing for potential precipitation in Lake Geneva and other nearby peri-alpine lakes (Dittrich et al., 2004; Escoffier et al., 2022; Groleau et al., 2000).

Calculating Ω_{CO2} at high frequency from sensor-derived pCO_2 timeseries (see Section 2.4.2), we then estimated at each time step the maximum depth of the calcite supersaturated layer where precipitation was thermodynamically achievable (i.e., $\Omega_{CO2} \leq 0.75$ corresponding to $\Omega_{CaCO3} \geq 2.5$). In practice, the first depth (from the surface) where $\Omega_{CO2} > 0.75$ was identified, and the compensation depth (i.e., where $\Omega_{CO2} = 0.75$) was calculated by linear interpolation using the above measuring depth and its corresponding Ω_{CO2} value.

This approach allowed us to resolve the thickness of the calcite supersaturated layer at each time step while coping with the effect of internal motions. Indeed, internal motions in Lake Geneva imply substantial vertical baroclinic dislocations (Fernández Castro et al., 2021) such that sensors at fixed depths may alternatively measure super- or undersaturated water layers with respect to calcite. Mean Alk in the calcite supersaturated layer was calculated from the sensor-derived Alk data above the compensation depth, so as to trace its decrease due to calcite precipitation. The corresponding mean Alk timeseries was then averaged daily and smoothed using a 5-days moving average window consistent with the main period of Kelvin waves in nearshore regions of Lake Geneva (Bouffard and Lemmin, 2013). Volumetric calcification rates were calculated as half the daily Alk mean rate of change, following the stoichiometry of the precipitation reaction (Eq. (2)).

$$Ca^{2+} + 2HCO_3^- \underset{Ks}{\leftrightarrow} CaCO_{3(s)} + CO_2 + H_2O \tag{2}$$
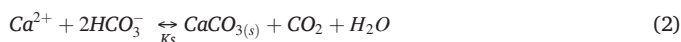
Areal calcification rates were determined in the same manner but using the daily rate of change of the Alk stock integrated between the surface and 30 m depth. Both volumetric and areal rates were additionally corrected for dilution effects as detailed in the next section.

2.4.4. Dilution by the Rhône River

During the stratified period, the propagation of snowmelt-diluted Rhône River water as an interflow through the lake's metalimnion can lower the Alk and ion concentrations in the surface layers (Halder et al., 2013). Therefore, additional correction was required to account for such an effect on the estimation of calcite precipitation rates. Following the approach by McConnaughey et al. (1994), discrete Mg^{2+} concentrations were used to normalize the estimated daily calcite precipitation rates, as (Eq. (3)):

$$Calcification(t) = \frac{dAlk/2}{dt} * \frac{[Mg^{2+}]avg}{[Mg^{2+}](t)} \tag{3}$$

where $[Mg^{2+}]avg$ corresponds to the average Mg^{2+} concentration in the lake (i.e., 240 μM) and $[Mg^{2+}](t)$ to the instant average concentration in surface layers. Mg^{2+} was selected because of its relatively conservative behavior; in Lake Geneva waters the molar ratio of Mg:Ca < 2 implies that Mg-bearing carbonate minerals should not precipitate (Stabel, 1986). We interpolated between Mg^{2+} measurements to estimate daily Mg^{2+} concentrations.

The coherence of this approach was also assessed by comparing the relative seasonal loss of Ca^{2+} estimated from areal calcite precipitation rates or derived from the temporal evolution of discrete Ca^{2+}/Mg^{2+} ratios calculated at each of the 6 measuring depths and integrated from the surface down to 30 m depth.

2.4.5. Net Ecosystem Production rate estimation

During periods of potential calcite precipitation, daily volumetric rates of NEP (mmol C m^{-3} d^{-1}) were calculated in the calcite supersaturated layer following Andersen et al. (2019), and according to (Eq. (4)):

$$NEPc(t) = \frac{dDIC}{dt} - Calcification(t) \pm FCO_2(t) \tag{4}$$

Daily calcification rates were determined according to the previous details. Daily DIC rates of change were computed from mean DIC in the supersaturated layer, which was, as with mean Alk, first calculated from hourly data before being averaged daily and smoothed over 5 days. Daily DIC rates were also corrected for dilution effects. The flux of CO_2 (FCO_2 in mmol m^{-2} h^{-1}) between the lake water and the atmosphere was calculated according to Perolo et al. (2021) as (Eq. (5)):

$$FCO_2(t) = k\,L\,\Delta pCO_2 \tag{5}$$

where k is the piston velocity (cm h^{-1}), L is the CO_2 solubility coefficient (mmol m^{-3} μatm^{-1}) and ΔpCO_2 is the partial pressure difference between the water and the atmosphere corrected for altitude (μatm). The piston velocity k was calculated according to the process-based model by Read et al. (2012) accounting for wind shear and convection derived from the local weather measurements at the LéXPLORE platform. The calculated fluxes were also corrected for chemical enhancement following Wanninkhof and Knox (1996). Hourly volumetric CO_2 fluxes were obtained by dividing the hourly areal fluxes by hourly values of the mixed layer depth.

The depth of the mixed layer was defined from the pycnocline depth, which was estimated whenever a minimum vertical temperature gradient of 0.5 °C m^{-1} could be identified in the water column. It was calculated from water density at an hourly timestep according to the formulas provided in Read et al. (2011), as was also estimated the maximum buoyancy frequency (i.e., N^2 max in s^{-2}). The hourly volumetric CO_2 fluxes were then summed over 24 h to obtain daily estimates and smoothed over 5 days to be consistent with the other terms used for NEP calculations.

3. Results

3.1. Timeseries overview

The time series of sensor measurements illustrated the typical seasonal patterns of surface layers in Lake Geneva (Fig. 2 & Fig. S2). In both 2019 and 2020, warming water temperatures (Fig. 2a) accompanied the establishment of stratification, with surface temperature increasing from ~15
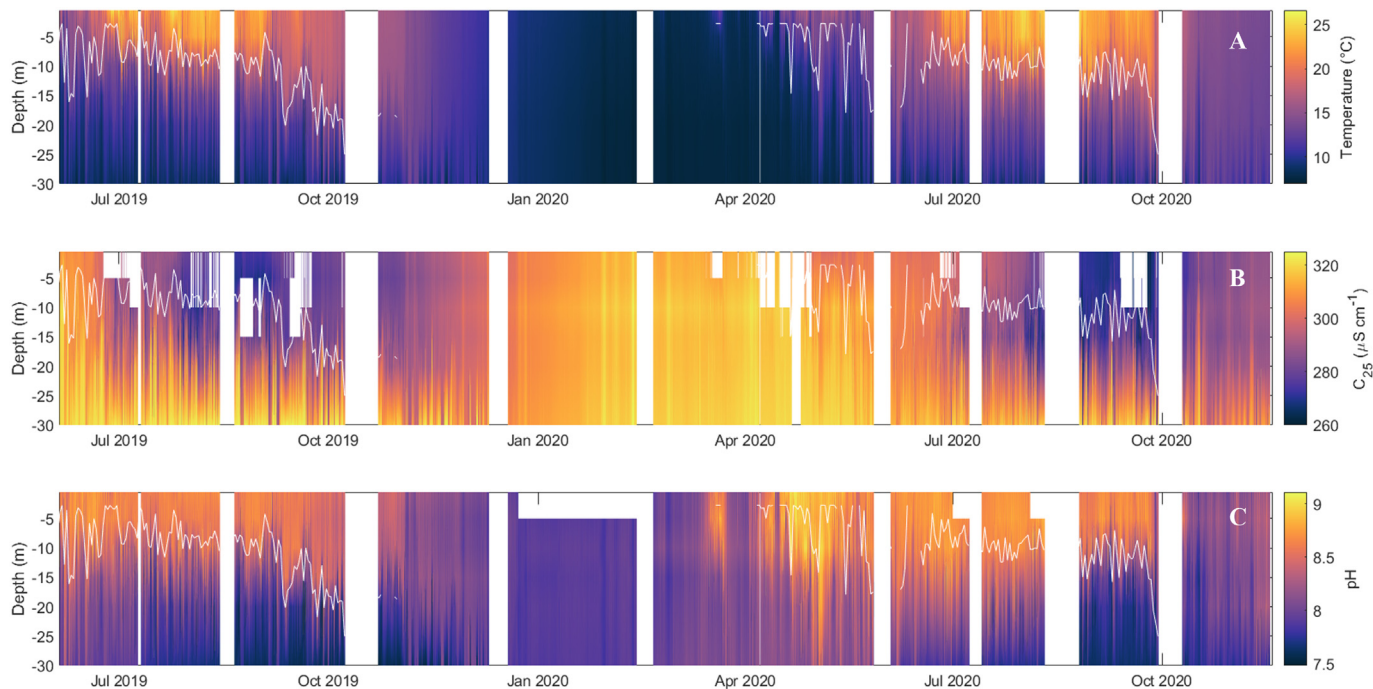
Fig. 2. Hourly averaged time series of temperature (a), specific conductance (b, C_{25}) and pH (c) data measured at 6 depths between 0.5 and 30 m at LéXPLORE from 04 June 2019 to 18 November 2020. Daily mixed layer depth (i.e., pycnocline depth) is indicated as a white line and was calculated whenever a minimum gradient of 0.5 $^\circ$C m^{-1} could be identified in the water column.

°C to maxima of ~25 °C during the stratified periods. At the end of spring, the mixed layer depth showed important vertical variations due to the weak strength of stratification. With warming surface conditions, the mixed layer depth became more stable and tended to deepen until early October in both years when the cooling of surface waters weakened the stratification. While incomplete for 2019, the dataset suggested a longer duration of the stratification in 2020. As a result, the mean mixed layer depth was deeper in 2020 compared to 2019, averaging respectively -9.8 ± 2.3 m and -8.7 ± 3.5 m for the summer period. Short-term variability was superimposed to the seasonal pattern, with strong vertical mixing events occurring on timescales from hours to days in response to wind-induced internal motions.

Specific conductance and pH followed clear seasonal trends on which short-term variability overlapped (Fig. 2b & c). Following the onset of stratification, pH values increased in the surface layers from a homogeneous winter value of ~7.9 to maximum average summer values between 8.6 and 8.7 during both years. A local maximum of ~9 was measured after spring overturn in 2020. Coincident with temperature and pH during stratification but slightly lagged, specific conductance values in the mixed layer decreased from a winter value of 320 µS cm^{-1} to values of ~270 and 260 µS cm^{-1} at the end of the summer 2019 and 2020, respectively. Interestingly, the concomitant pH increase and specific conductance decrease occurred deeper than the mixed layer depth during both years. In 2019, these patterns were observed down to ~15 m during summer while, for 2020, they occurred down to ~20 m. At the end of the stratification periods, pH and specific conductance decreased and increased, respectively, with values becoming more homogeneous at all depths.

3.2. Tracing alkalinity from specific conductance

Alk data from discrete samples were strongly linearly correlated with specific conductance (p < 0.001; Fig. S3a), so that high-frequency data could be used as a proxy of the Alk dynamics in surface waters. Moreover, the highly significant correlation between discrete Alk and Ca^{2+} concentrations (p < 0.001; Fig. S3b), and especially the value of the slope, indicated that calcite precipitation was the main process underlying the Alk dynamics

(i.e., slope = 0.55 +/− 0.02, consistent with the loss of two moles of Alk (i.e., HCO$_3^-$) for one mole of Ca^{2+} during precipitation; Eq. (2)).

The integration of the sensor-derived Alk data in the top 30 m of the lake was used to describe the temporal dynamics of the total Alk stock during the study period (Fig. 3). Daily estimates showed a substantial decrease of the Alk stock during the stratified periods of both years, from initial values of ~48 mol m^{-2}, after spring overturn, to minimum values of ~41 and ~39 mol m^{-2} in 2019 and 2020, respectively. In both years, periods of progressive decline in the Alk stock were interspersed with short-term plateaus or slight increase associated with higher daily variability (e.g., in early July 2019). High daily variability was also observed at the end of the stratified periods in both years when the shouldering of the Alk stock values preceded their subsequent increase.

Coincident observations of the Mg^{2+} concentration dynamics in the top 30 m of the lake indicated that the apparent Alk stock losses of ~7 and ~9 mol m^{-2} in 2019 and 2020, respectively, were not solely related to calcite precipitation. As for other ions, the average Mg^{2+} concentration decreased by ~5 % during stratification compared to its initial value at spring overturn (Fig. S4). This decrease cannot be attributed to the precipitation of Mg-bearing carbonate minerals. Instead, it reflects the influence of the snow- and glacier-melt diluted Rhône River waters that propagate as an interflow in the lake's metalimnion and progressively accumulate in surface layers during the stratified season.

Accounting for such an effect, the maximum Alk stock loss due to calcite precipitation amounted to ~5 and ~7 mol m^{-2} in 2019 and 2020, respectively, corresponding to ~30 and ~42 gC m^{-2} precipitated as inorganic carbon. Importantly, for the 2020 stratified period, the sensor-derived flux was in close agreement with the cumulative total particulate inorganic carbon flux measured from sediment traps (Fig. 4).

3.3. Depth-resolved dynamics of calcite precipitation

The similar flux measured at 10 and 30 m depth from sediment traps (Fig. 4) as well as the dynamics of Ca^{2+}/Mg^{2+} molar ratios (Fig. S5) indicated that the overall Alk stock losses resulted from calcite precipitating
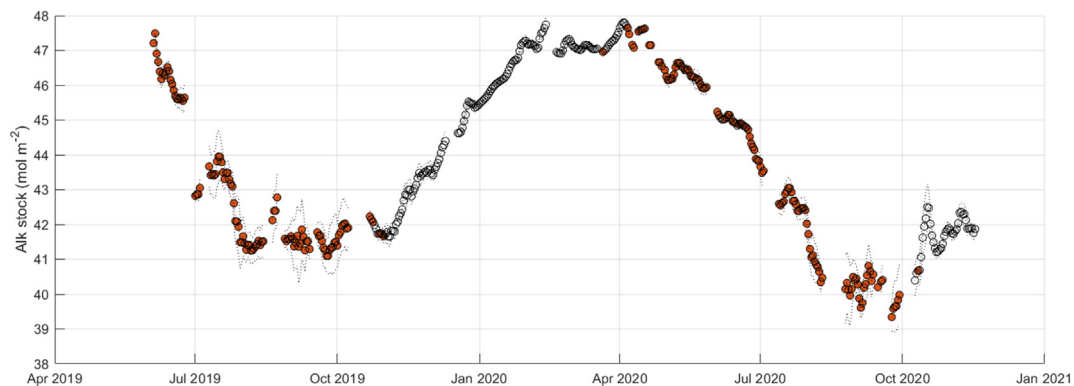
Fig. 3. Temporal dynamics of the Alk stock (in mol m^{-2}) integrated between the 0.5 and 30 m depths, and estimated from specific conductance sensor data. Smoothed daily averaged Alk stock values are represented as circles while black dashed-lines correspond to daily standard deviation. Orange-colored circles identify the periods of water column stratification.

mainly in the uppermost part of the water column. This observation is consistent with the time-resolved depth of the calcite supersaturated layer, which extended from the surface down to -10.5 ± 2.6 m and -13.3 ± 3.3 m during the summer periods of 2019 and 2020, respectively (Fig. 5 & Fig. S6). These results support the observations that water layers contributing to calcite precipitation extended below the mixed layer depth (Fig. 2 in Section 3.1). However, the substantial vertical variability of these layers at short timescales also showed that they typically overlapped and mixed over the temporal window considered for our calculations. The Alk levels in the calcite supersaturated layer were remarkably homogenous, as illustrated by the temporal evolution of the corresponding average Alk and its moderate variability across depths (Fig. 6a). Such a dynamic was characterized by an overall decrease of the average Alk during the stratified seasons with values ranging between 1565.2 ± 24.5 μM and 1269.3 ± 11.5 μM in 2019 and between 1611.8 ± 5.8 μM and 1245.6 ± 7.9 μM in 2020. Accounting for the dilution by the Rhône interflow, the minimum average Alk represented a seasonal loss of ∼15 % and ∼20 % compared to the initial level at the beginning of summer or spring overturn in 2019 and 2020, respectively.

Periods of increasing water column stability (e.g., in July – August of both years, Fig. 6a) corresponded with high Alk losses due to calcite
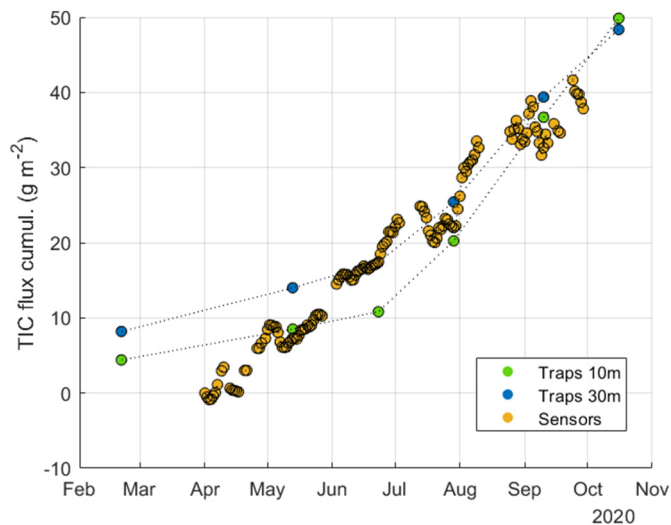
Fig. 4. Cumulative total particulate inorganic carbon flux (gC m^{-2}) measured from sediment traps deployed at the 10 m (green points) and 30 m (blue points) depths at LéXPLORE in 2020 or estimated from the sensor-derived dilution-corrected Alk stock loss in the top 30 m during stratification.

precipitation (Fig. 6b). Maximum daily calcite precipitation rates computed from dilution-corrected Alk loss (i.e., ∼9 and ∼8.1 mmol C m^{-3} d^{-1}, in 2019 and 2020, respectively) were associated with local maxima of the water column stability (i.e., ∼3 10^{-3} s^{-2} and 2.2 10^{-3} s^{-2} in 2019 and 2020, respectively; Fig. S7). Lower values were mostly calculated at the beginning and end of the stratified periods. Estimated daily calcite precipitation rates averaged 2.2 ± 1.9 mmol C m^{-3} d^{-1} in 2019 and 1.8 ± 1.9 mmol C m^{-3} d^{-1} in 2020.

3.4. Calcite precipitation and Net Ecosystem Production

Former observations showed that periods of calcite precipitation and stratification coincided with depleted surface CO_2 concentrations and undersaturated pCO_2 values (Fig. 5). Despite these conditions, substantial levels of autotrophic metabolism were maintained (Fig. 7). During summer 2019, maximum NEP values occurred at the end of June and end of August, ranging between ∼8.5 and 15 mmol C m^{-3} d^{-1} (Fig. 7b). In 2020, summer maximum NEP values were slightly lower (i.e., ∼8.5 mmol C m^{-3} d^{-1}) while higher maximum values (i.e., ∼14 mmol C m^{-3} d^{-1}) were observed both in spring and early autumn. Autotrophic metabolism corresponded to substantial amounts of DIC removed from the water column (Fig. 7a). However, the speciation and origin of the removed DIC varied across the periods and years considered. At the beginning of summer 2019 and in spring 2020, the total DIC removed included a higher contribution of CO_2 derived from the inward atmospheric flux (i.e., reaching maximum values of ∼5 mmol m^{-3} d^{-1} in both situations), while the magnitude of this flux decreased during summer in both years (i.e., averaging ∼2.5 mmol m^{-3} d^{-1}). Concomitant with this decrease during high water column stability, the increasing quantity of DIC removed to support summer NEP had to originate from another inorganic carbon species. Coincident maxima of summer NEP and calcite precipitation rates during both years suggest that the additional DIC was withdrawn from the Alk pool. Periods of increasing summer NEP values were coupled to increasing calcite precipitation rates, so that calcite precipitation to NEP molar ratios increased accordingly (Fig. 7b-c). Over the whole study period, calcite precipitation to NEP molar ratios averaged 0.39 ± 0.24 (or 0.56 when estimated from the slope of the linear correlation between daily estimates of NEP and DIC, Fig. S8a). Considering each year separately, the average calcite precipitation to NEP molar ratio was 0.43 ± 0.23 in 2019 and 0.37 ± 0.24 in 2020 (or 0.57 in 2019 and 0.37 in 2020 from respective linear correlations, Fig. S8b). However, fine-scale daily observations indicated that calcite precipitation to NEP molar ratios reached maximum values of 1:1 during periods of high productivity (Fig. 7c). Interestingly, these periods corresponded to windows of decreasing CO_2 concentrations in the calcite supersaturated layer (i.e., reaching values as low as ∼6 μM), indicating that local maxima of the molar ratios coincided with enhanced calcite supersaturation levels in surface waters.
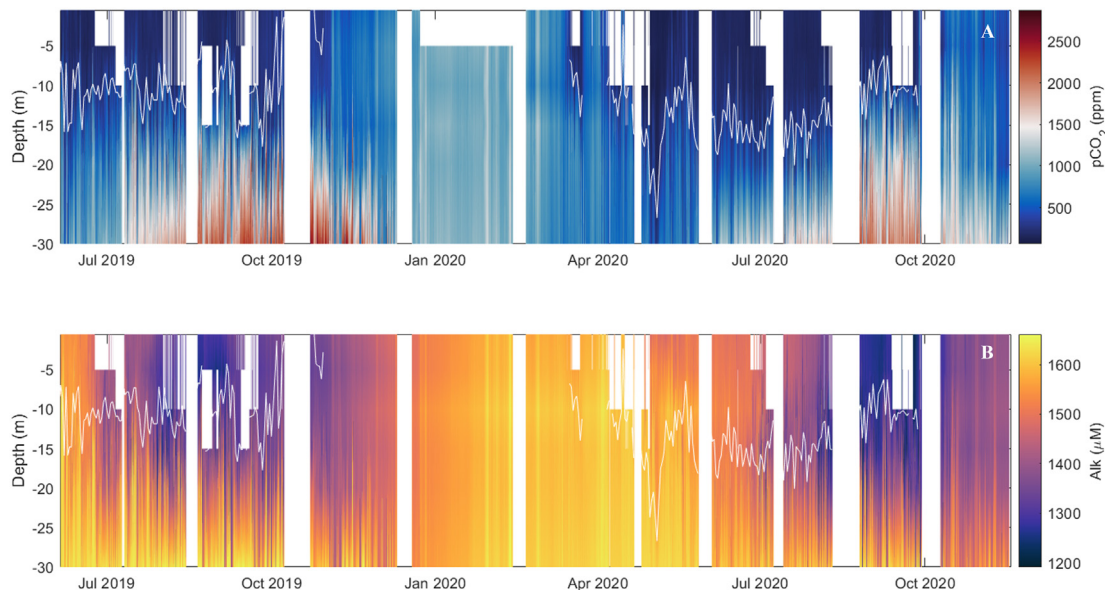
Fig. 5. Hourly time series of pCO$_2$ (a) and Alk (b) between 0.5 and 30 m depth at LéXPLORE from 04 June 2019 to 18 November 2020. The white line represents the average daily lower depth of the calcite supersaturated layer.

4. Discussion

The present study provides a detailed analysis of the dynamics of calcite precipitation in the surface layers of the deep basin of Lake Geneva. Specifically, it (*i*) assesses the relevance of using high-frequency multi-sensor data to trace calcite precipitation, (*ii*) estimates the magnitude of the process at different time scales (day to season) and evaluates its significance for the lacustrine carbon budget, and (*iii*) investigates fine-scale coupling between pelagic calcite precipitation and primary production in the lake surface waters.

4.1. Calcite precipitation from high-frequency data

The correlation between sensor and discrete sample measurements supported the use of high-frequency specific conductance data as a proxy of Alk dynamics in surface waters. However, several conditions had to be fulfilled to strictly relate Alk variations to calcite precipitation.

In freshwater systems, Alk is commonly expressed as the sum of [HCO$_3^-$] + 2[CO$_3^{2-}$] (Michard, 2002), but this simplification may be biased by the occurrence of substantial concentrations of HS$^-$ and S^{2-}. The well oxygenated surface layers of Lake Geneva prevent the formation of
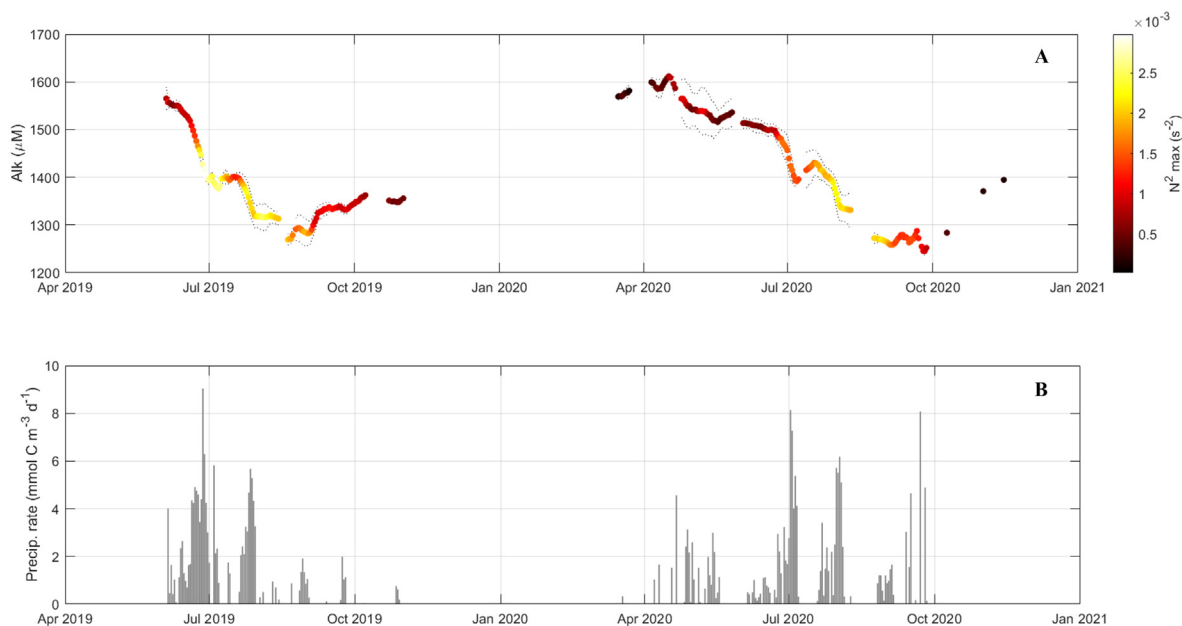

Fig. 6. (a) Temporal dynamics of the daily average Alk (μM) in the calcite supersaturated layers in 2019 and 2020. Daily Alk values are represented by circles colored according to the corresponding daily averaged value of the maximum buoyancy frequency N^2 (s^{-2}) at the pycnocline depth. Black dashed-lines represent the daily Alk standard deviation. (b) Daily calcite precipitation rates (mmol C m^{-3} d^{-1}) computed from daily variation in the dilution-corrected average Alk in the calcite supersaturated layer (i.e., half the daily rate of change of data in (a)).
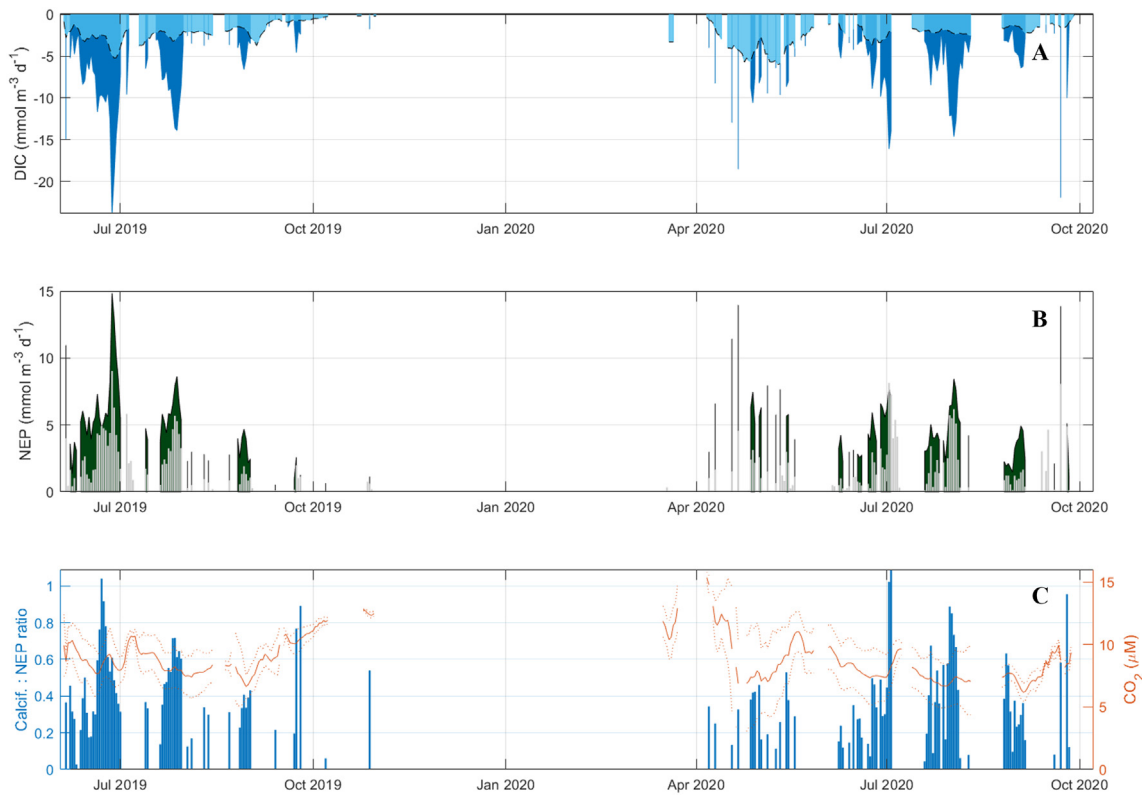
Fig. 7. (a) Daily values of the total DIC removed (in dark blue) from the calcite-supersaturated layer with contribution from the inward daily atmospheric CO_2 flux over the study period represented as a shaded area (in light blue). (b) Daily NEP rates (mmol C m^{-3} d^{-1}) in the calcite-supersaturated layer (in dark green) on which daily calcite precipitation rates (from Fig. 6b) have been superimposed (in light grey). (c) Daily calcite precipitation rates to NEP molar ratios computed from the estimates in (b) and temporal dynamics of the daily average CO_2 concentration in the calcite supersaturated layer (mean $\pm$ SD as solid and dashed orange lines, respectively).

these latter compounds, thereby corroborating the common expression of Alk. Moreover, considering the pH of Lake Geneva surface waters (i.e., ~ 7.9–9), bicarbonate ions are predominant over carbonate ions, and Alk can be approximated as ~ $[HCO_3^-]$. Furthermore, the value of the linear slope relating Ca^{2+} and Alk was consistent with the stoichiometry of the calcite precipitation reaction (Eq. (2)), supporting that specific conductance was used as a tracer of the process.

The link between specific conductance and Alk is a common feature in hardwater lakes (Andersen et al., 2017; Müller et al., 2016), which derives from carbonate or silicate weathering in the catchment (Marcé et al., 2015; Zobrist et al., 2018). Specific conductance may hence allow tracing major ions such as Ca^{2+} and bicarbonates, but additional caution is required. As previously observed (McConnaughey et al., 1994), our data showed that snow- and ice-melt waters can significantly dilute ion concentrations in the lake. To infer biogeochemical dynamics from high-frequency data, such effects must be taken into account.

Our approach to integrating the depth-resolved dynamics of calcite precipitation derived from previous investigations describing the effects of internal waves on lake metabolism estimation from high-frequency DO data (Fernández Castro et al., 2021). Moreover, building on additional geochemical observations (Müller et al., 2016), we used the relationship between Ω_{CO2} and Ω_{CaCO3} in Lake Geneva to define the calcite supersaturated layer susceptible to precipitation. The relevance of this method was supported by the pH values in the calcite supersaturated layer, which were equal to or higher than the theoretical pH of water in equilibrium with calcite and atmospheric pCO_2 (i.e., ~ 8.32; Michard, 2002).

Beyond identifying the calcite supersaturated layer, accurate quantification of calcite precipitation depended on the isolation and extent of mixing of this layer with deeper waters. The depth of the calcite supersaturated layer was generally slightly higher than the pycnocline depth during both years, likely corresponding to the lower edge of the metalimnion. During

stable stratified conditions, strong density gradients in the metalimnion imply the prevalence of slow molecular diffusion, which can be neglected regarding the mixing of dissolved species (Groleau et al., 2000). In contrast, during periods of weak stratification, vertical turbulent diffusion may bias the estimation of calcite precipitation from apparent Alk loss in the supersaturated layer due to its mixing with more concentrated hypolimnetic waters. This probably occurred at stratification onset in late spring or early summer and prevented quantifying calcite precipitation during transient mixing events in July 2019 and July 2020. This effect could restrict our approach outside periods of stratification, but corresponding calcite supersaturation windows were not identified during the study. Thus, while turbulent mixing processes may have affected the accuracy of our estimates, previous findings in Lake Geneva (Fernández Castro et al., 2021) indicate that such an effect was negligible during stratification. Moreover, the close correspondence between sensor-derived TIC flux and sediment trap estimates in 2020 (Fig. 4) supports the reliability of our approach to trace calcite precipitation in Lake Geneva.

4.2. Dynamics of calcite precipitation and relevance for the carbon budget

Calcite precipitation in hardwater lakes has mostly been studied using coarse-scale methodological approaches. The proposed methodology provides novel insights into the environmental conditions supporting the dynamics of calcite precipitation at distinct time scales.

Alk loss in Lake Geneva in 2019 and 2020 occurred during the warm stratified seasons when CO_2 was depleted in surface waters. Over the summer season, areal calcite precipitation rates (i.e., ~ 30 and ~ 42 gC m^{-2} in 2019 and 2020) were in close agreement with former estimates for Lake Geneva (Dominik et al., 1993; Perga et al., 2016). In contrast, our results are higher than fluxes measured in high-altitude lakes (Ohlendorf and Sturm, 2001) or in the Great Lakes area (Hodell et al., 1998) and lower than values

reported for Lake Constance (Stabel, 1986) and hardwater lakes from the Swiss Plateau (Müller et al., 2016) or nearby regions (Groleau et al., 2000; Perga et al., 2016).

While these differences may result from methodological inconsistencies and limitations (e.g., advection of detrital material in sediment traps or cores, dissolution of calcite induced by organic matter mineralization, and hydrological uncertainties in mass-balance calculations), they may also reflect fundamental features in the functioning of lacustrine systems. As conceptualized by Müller et al. (2016), calcite precipitation in hardwater lakes may depend both on total P (TP) concentrations and Alk levels in surface waters at spring overturn. By stimulating primary production, higher TP concentrations may enhance CO_2 removal and calcite supersaturation. Areal estimates of calcite precipitation in the oligo-mesotrophic Lake Geneva support this assertion as they generally position above oligotrophic (Hodell et al., 1998; Ohlendorf and Sturm, 2001) and below meso- to eutrophic values (Müller et al., 2016). Yet, the relationship between CO_2 and TP may be non-monotonic such that effects on calcite precipitation may be more complex (Perga et al., 2016). Surface Alk at spring overturn is another fundamental parameter as it determines the amount of calcite that can precipitate before the lake water reaches equilibrium with calcite and atmospheric CO_2 (i.e., equilibrium Alk ~1200 μM). The spring Alk in Lake Geneva (~ 1700 μM) confirms that above the equilibrium value lakes are prone to calcite precipitation (Marcé et al., 2015). Moreover, the magnitude of seasonal Alk losses in 2019 and 2020 (i.e., ~ 15 % and ~20 % of spring levels, respectively) supports theoretical predictions that a maximum of 30 % of Alk may be precipitated as calcite (Müller et al., 2016). Our results and previous ones (Dominik et al., 1993), nevertheless, illustrate the interannual variability in the magnitude of calcite precipitation, indicating that additional environmental factors constrain the process.

Water temperature is an important driving condition as it affects the solubility of calcite and saturation state of the water as well as the stratification of the lake (Hodell et al., 1998). The differences in seasonal areal precipitation rates between 2019 and 2020 did not correspond with varying maximum water temperatures but could be related to distinct patterns of water column stratification. The higher seasonal calcite precipitation observed in 2020 was not associated with the strength of stratification, as maximum N^2 stability occurred in 2019 (Fig. S7b). It could rather be related to the duration of lake stratification. Though data are incomplete for 2019, our results suggest a longer period of stratification in 2020, which translated into a deeper pycnocline and depth of the calcite supersaturated layer (Fig. 2 & Fig. 5). This observation explains that, despite similar average daily volumetric rates of calcite precipitation in the two years (i.e., 2.2 ± 1.9 and 1.8 ± 1.9 mmol C m^{-3} d^{-1} in 2019 and 2020, respectively), more Alk was lost in 2020 because calcite precipitation occurred from a larger water volume. Similar observations were made in Lake Ontario, indicating more calcite precipitation during warm years with earlier seasonal stratification (Hodell et al., 1998). This increase in precipitation was, additionally, reflected in the higher δ^{13}C-DIC, which is illustrative of the greater volumetric CO_2 removal by photosynthesis. Importantly, in Lake Geneva the magnitude of seasonal inorganic C loss as calcite from the top 30 m in 2019 and 2020 (i.e., ~ [30–42] g C m^{-2}) was similar to the amount of organic C produced by NEP in 2019 (i.e., [50–89] g C m^{-2}; Fernández Castro et al., 2021). This highlights the major contribution of the inorganic component to the cycling of C in lake surface waters during stratification. Moreover, the fate of these distinct forms of particulate C in the water column may have important implications for the dynamics of the whole lake C cycle. Organic C may be more prone to remineralization in the water column than calcite to dissolution during settling, leading to a greater net accumulation of inorganic rather than organic C in the sediments (Müller et al., 2016). However, net organic C burial may still occur (Dominik et al., 1993) and its subsequent remineralization may create the conditions for benthic calcite dissolution (Megard, 1968; Müller et al., 2006). These combined processes may hence affect spatially and temporally the translocation between particulate and dissolved phases as well as the speciation of C in the lake. Furthermore, the regeneration of DIC produced in bottom sediments to surface waters may act as a carbonate counter pump whose

relevant time scales depend on the depth and mixing regime of the system (Andersen et al., 2017).

Beyond refining the seasonal contribution of calcite precipitation to the lacustrine C budget, we documented the fine scale variability and magnitude of the process. Maximum daily calcite precipitation rates (i.e., ~ 9 and ~8.1 mmol C m^{-3} d^{-1}, in 2019 and 2020, respectively) were near the upper range of the few reported estimates (Khan et al., 2022). These observations may derive from the inherent averaging effect of the methodologies used to study calcite precipitation but also indicate that short-term variability responds to dynamic environmental controls.

4.3. Coupling between calcite precipitation and primary production

The relationship between calcite precipitation and primary production has commonly been considered through the lens of pH increase due to CO_2 assimilation that enhances the supersaturation of waters with respect to calcite (Stabel, 1986). Our detailed observations support this coupling and provide additional insights into its fine scale dynamics in a deep hardwater lake.

Calcite precipitation and NEP have been related through their molar ratios, noted as α hereafter, which allow accounting for the relative contributions of both processes on the total DIC removed from the water. At the seasonal scale, α values for 2019 and 2020 (i.e., ~ [0.35–0.55]) are within the range of values reported for littoral habitats and shallow lakes (i.e., [0.3–0.7]; Andersen et al., 2019; McConnaughey et al., 1994), while slightly exceeding the few available pelagic estimates (i.e., [0.25–0.4]; Megard, 1968). These values are reflected in the ratio between seasonal areal precipitation in 2019 (i.e., ~ 30 g C m^{-2}) and DO-derived NEP in the top 30 m (i.e., [50–89] g C m^{-2}; Fernández Castro et al., 2021) and, therefore, support the relevance of our estimates. These results, moreover, indicate that a third to a half of the DIC fixed as NEP during summer derives from calcite precipitation. The consistent range of pelagic α estimates in Lake Geneva and other lakes may partly result from geochemical constraints linked to the maintenance of calcite supersaturation (Megard, 1968) or Alk surface level (e.g., α hypothesized as = 0.2 for Alk between 1 and 2.23 meq L^{-1}; Khan et al., 2020). However, additional insight into the mechanisms supporting α values may be derived from their fine scale dynamics, which reflect the interplay between DIC availability, speciation, and intensity of primary production.

Our study documented a dynamic coupling between processes, with increasing rates of calcite precipitation during periods of increasing water column stability, coinciding with maximum NEP and α ratios (Fig. 7). This indicates that during stable periods of limited atmospheric and hypolimnetic exchange, increasingly more DIC was extracted from the Alk pool to support primary production such that calcite precipitation and NEP rates eventually reached equimolar values. This finding supports the previously reported positive relationship between calcite saturation level and α (Khan et al., 2021), as illustrated by the concurrent decrease in surface CO_2 concentrations and increase in α ratios (Fig. 7c). Moreover, it enables comparisons with the mechanisms observed in shallow macrophyte-dominated lakes, where dynamic α ratios have been documented, both seasonally and daily (Andersen et al., 2019; McConnaughey et al., 1994).

The α value reflects the relative allocation of C between organic biomass and calcite. It depends on the balance between photosynthesis without calcification, which raises pH without affecting Alk, and photosynthesis accompanied by precipitation, which decreases Alk without modifying pH (Sand-Jensen et al., 2021). As shown from mesocosm experiments (Hammer et al., 2019), in hardwater lakes of intermediate to high DIC concentrations, the initial consumption of net available CO_2 by the former photosynthetic process elevates pH so that DIC from both chemically enhanced atmospheric uptake and calcite precipitation may additionally be supplied to NEP. However, as Alk is increasingly eroded by calcite precipitation and pH stabilized, the decrease in carbonate buffering capacity reduces the efficiency of atmospheric uptake, enhancing the relative importance of precipitation for NEP and hence the α value. These patterns are consistent with observations made in Lake Geneva but may differ with

regard to relevant time scales compared to shallower environments. In shallow lakes, higher photosynthetic rates favored by diel convective DIC replenishment may constrain this succession of processes to the sub-daily scale (Andersen et al., 2019).

In both environments, these mechanisms buffer pH below detrimental levels for photosynthesis, as confirmed in Lake Geneva. Yet, in macrophyte-dominated lakes calcification is recognized as a controlled process, while in deeper hardwater systems, it is considered a passive one generally induced by picocyanobacteria (Dittrich and Obst, 2004; Hodell et al., 1998). The precipitation of calcite in Lake Geneva may, hence, be simply triggered by the photosynthetic activity of picocyanobacteria, which can dominate phytoplankton productivity during stratification (Parvathi et al., 2014). Conversely, the precipitation process may respond to a controlled mechanism relying on intracellular amorphous calcium carbonate inclusions found to be widespread among cyanobacteria (Benzerara et al., 2014) and uncovered in nano-eukaryotes from the Petit-Lac (Martignier et al., 2017). Owing to the prevalent CO_2-concentrating mechanisms developed by autotrophs in alkaline systems (Maberly and Gontero, 2017), these considerations, along with the dynamic coupling with NEP, challenge the non-controlled nature of pelagic calcite precipitation.

5. Conclusions

The present study showed that high frequency multi-sensor data provides an accurate approach for tracing pelagic calcite precipitation in a large hardwater lake, Lake Geneva. We quantified the magnitude of the process over two annual cycles, and described the underlying macroscopic environmental drivers. In particular, our results supported previous observations that the level of Alk, trophic state, and the duration of water column stratification are major determinants of calcite precipitation at the seasonal scale. We found that calcite precipitation is an important contributor to the whole-lake C budget. At a finer scale, our results highlighted the tenuous link between organic and inorganic C processes revolving around calcite precipitation. The fine temporal resolution of our approach revealed a marked daily variability in calcite precipitation, which was tightly coupled with the dynamics of pelagic autotrophic metabolism. Beyond quantifying daily calcite precipitation rates and their stochiometric ratios with NEP, our analyses indicated an increased coupling of both processes during conditions of increasing water column stability. Such pattern resulted from the enhanced extraction of DIC from the Alk pool by primary production during stable conditions, thereby raising the question of whether pelagic calcite precipitation is only induced by increasing calcite saturation during bicarbonate-based photosynthesis or is more actively controlled. Elucidating these mechanisms and the fate of the inorganic C precipitated as calcite are next critical steps towards deepening our knowledge of the biogeochemical cycling of C in lakes.

CRediT authorship contribution statement

Nicolas Escoffier: Conceptualization, Methodology, Data curation, Formal analysis, Investigation, Writing – original draft, Writing – review & editing. **Pascal Perolo:** Investigation, Writing – review & editing. **Gaël Many:** Investigation, Writing – review & editing. **Natacha Tofield Pasche:** Investigation, Writing – review & editing. **Marie-Elodie Perga:** Conceptualization, Funding acquisition, Project administration, Writing – review & editing.

Data availability

Processed data at LéXPLORE are available on Zenodo (https://doi.org/10.5281/zenodo.7463768). Pluri-annual monitoring data at SHL2 are openly available in IS OLA (Observatory on LAkes) at https://si-ola.inrae.fr/si_lacs/.

Declaration of competing interest

The authors declare that they have no known competing financial interests or personal relationships that could have appeared to influence the work reported in this paper.

Appendix A. Supplementary data

Supplementary data to this article can be found online at https://doi.org/10.1016/j.scitotenv.2022.160699.

References

Andersen, Mikkel R., Kragh, T., Sand-Jensen, K., 2017. Extreme diel dissolved oxygen and carbon cycles in shallow vegetated lakes. Proc. R. Soc. B Biol. Sci. 284 (1862). https://doi.org/10.1098/rspb.2017.1427.

Andersen, Mikkel René, Kragh, T., Martinsen, K.T., Kristensen, E., Sand-Jensen, K., 2019. The carbon pump supports high primary production in a shallow lake. Aquat. Sci. 81 (2), 1–11. https://doi.org/10.1007/s00027-019-0622-7.

Benzerara, K., Skouri-Panet, F., Li, J., Férard, C., Gugger, M., Laurent, T., 2014. Intracellular Ca-carbonate biomineralization is widespread in cyanobacteria. Proc. Natl. Acad. Sci. U. S. A. 111 (30), 10933–10938. https://doi.org/10.1073/pnas.1403510111.

Bouffard, D., Lemmin, U., 2013. Kelvin waves in Lake Geneva. J. Great Lakes Res. 39 (4), 637–645. https://doi.org/10.1016/j.jglr.2013.09.005.

Cole, J.J., Prairie, Y.T., Caraco, N.F., McDowell, W.H., Tranvik, L.J., Striegl, R.G., et al., 2007. Plumbing the global carbon cycle: integrating inland waters into the terrestrial carbon budget. Ecosystems 10 (1), 171–184. https://doi.org/10.1007/s10021-006-9013-8.

Dittrich, M., Obst, M., 2004. Are picoplankton responsible for calcite precipitation in lakes? Ambio 33 (8), 559–564. https://doi.org/10.1579/0044-7447-33.8.559.

Dittrich, M., Kurz, P., Wehrli, B., 2004. The role of autotrophic picocyanobacteria in calcite precipitation in an oligotrophic lake. Geomicrobiol J. 21 (1), 45–53. https://doi.org/10.1080/01490450490253455.

Dominik, J., Dulinski, M., Daniel, S., Hofmann, A., Favarger, P.-Y., Vernet, J.-P., 1993. Transfert de matière et de radio-isotopes entre l'eau et les sédiments dans le Léman. Rapport CIPEL Campagne 1992, pp. 163–188.

Duarte, C.M., Prairie, Y.T., 2005. Prevalence of heterotrophy and atmospheric CO2 emissions from aquatic ecosystems. Ecosystems 8, 862–870. https://doi.org/10.1007/s10021-005-0177-4.

Effler, S.W., Peng, F., 2012. Light-scattering components and secchi depth implications in onondaga Lake, New York, USA. Fundam. Appl. Limnol. 179 (4), 251–265. https://doi.org/10.1127/1863-9135/2012/0177.

Escoffier, N., Perolo, P., Lambert, T., Rüegg, J., Odermatt, D., Adatte, T., et al., 2022. Whiting events in a large peri-alpine lake: evidence of a catchment-scale process. J. Geophys. Res. Biogeosci. 127 (4). https://doi.org/10.1029/2022JG006823.

Fernández Castro, B., Chmiel, H.E., Minaudo, C., Krishna, S., Perolo, P., Rasconi, S., Wüest, A., 2021. Primary and net ecosystem production in a large lake diagnosed from high-resolution oxygen measurements. Water Resour. Res. 57 (5). https://doi.org/10.1029/2020WR029283.

Finlay, K., Leavitt, P.R., Wissel, B., Prairie, Y.T., 2009. Regulation of spatial and temporal variability of carbon flux in six hard-water lakes of the northern Great Plains. Limnol. Oceanogr. 54 (6 PART 2), 2553–2564. https://doi.org/10.4319/lo.2009.54.6_part_2.2553.

Gattuso, J.P., Allemand, D., Frankignoulle, M., 1999. Photosynthesis and calcification at cellular, organismal and community levels in coral reefs: a review on interactions and control by carbonate chemistry. Am. Zool. 39 (1), 160–183. https://doi.org/10.1093/icb/39.1.160.

Gaudard, A., Schwefel, R., Räman Vinnä, L., Schmid, M., Wüest, A., Bouffard, D., 2017. Optimizing the parameterization of deep mixing and internal seiches in one-dimensional hydrodynamic models: a case study with simstrat v1.3. Geosci. Model Dev. 10 (9), 3411–3423. https://doi.org/10.5194/gmd-10-3411-2017.

del Giorgio, P.A., Cole, J.J., Caraco, N.F., Peters, R.H., 1999. Linking planktonic biomass and metabolism to net gas fluxes in northern temperate lakes. Ecology 80 (4), 1422–1431.

Graham, N.D., Bouffard, D., Loizeau, J.L., 2016. The influence of bottom boundary layer hydrodynamics on sediment focusing in a contaminated bay. Environ. Sci. Pollut. Res. 23 (24), 25412–25426. https://doi.org/10.1007/s11356-016-7715-9.

Groleau, A., Sarazin, G., Vinçon-Leite, B., Tassin, B., Quiblier-Llobéras, C., 2000. Tracing calcite precipitation with specific conductance in a hard water alpine Lake (Lake Bourget). Water Res. 34 (17), 4151–4160. https://doi.org/10.1016/S0043-1354(00)00191-3.

Halder, J., Decrouy, L., Vennemann, T.W., 2013. Mixing of Rhône River water in Lake Geneva (Switzerland-France) inferred from stable hydrogen and oxygen isotope profiles. J. Hydrol. 477, 152–164. https://doi.org/10.1016/j.jhydrol.2012.11.026.

Hammer, K.J., Kragh, T., Sand-Jensen, K., 2019. Inorganic carbon promotes photosynthesis, growth, and maximum biomass of phytoplankton in eutrophic water bodies. Freshw. Biol. 64 (11), 1956–1970. https://doi.org/10.1111/fwb.13385.

Hodell, D.A., Schelske, C.L., Fahnenstiel, G.L., Robbins, L.L., 1998. Biologically induced calcite and its isotopic composition in Lake Ontario. Limnol. Oceanogr. 43 (2), 187–199. https://doi.org/10.4319/lo.1998.43.2.0187.

van Heuven, S., Pierrot, D., Rae, J.W.B., Lewis, E., Wallace, D.W.R., 2011. MATLAB Program Developed for CO2 System Calculations. ORNL/CDIAC-105b. Carbon Dioxide Information Analysis Center, Oak Ridge National Laboratory, U.S. Department of Energy, Oak Ridge, Tennessee https://doi.org/10.3334/CDIAC/otg.CO2SYS_MATLAB_v1.1.

van Hoek, W.J., Wang, J., Vilmin, L., Beusen, A.H.W., Mogollón, J.M., Müller, G., et al., 2021. Exploring spatially explicit changes in carbon budgets of Global River basins during the 20th century. Environ. Sci. Technol. 55 (24), 16757–16769. https://doi.org/10.1021/acs.est.1c04605.

Homa, E.S., Chapra, S.C., 2011. Modeling the impacts of calcite precipitation on the epilimnion of an ultraoligotrophic, hard-water lake. Ecol. Model. 222 (1), 76–90. https://doi.org/10.1016/j.ecolmodel.2010.09.011.

Khan, H., Laas, A., Marcé, R., Obrador, B., 2020. Major effects of alkalinity on the relationship between metabolism and dissolved inorganic carbon dynamics in lakes. Ecosystems https://doi.org/10.1007/s10021-020-00488-6.

Khan, H., Laas, A., Marcé, R., Sepp, M., Obrador, B., 2021. Eutrophication and geochemistry drive pelagic calcite precipitation in lakes. Water 13 (5). https://doi.org/10.3390/w13050597.

Khan, H., Marcé, R., Laas, A., Obrador Sala, B., 2022. The relevance of pelagic calcification in the global carbon budget of lakes and reservoirs. Limnetica 41 (1). https://doi.org/10.23818/limn.41.02.

Maberly, S.C., Gontero, B., 2017. Ecological imperatives for aquatic CO2-concentrating mechanisms. J. Exp. Bot. 68 (14), 3797–3814. https://doi.org/10.1093/jxb/erx201.

Marcé, R., Obrador, B., Morguí, J.A., Lluís Riera, J., López, P., Armengol, J., 2015. Carbonate weathering as a driver of CO2 supersaturation in lakes. Nat. Geosci. 8 (2), 107–111. https://doi.org/10.1038/ngeo2341.

Martignier, A., Pacton, M., Filella, M., Jaquet, J.M., Barja, F., Pollok, K., et al., 2017. Intracellular amorphous carbonates uncover a new biomineralization process in eukaryotes. Geobiology 15 (2), 240–253. https://doi.org/10.1111/gbi.12213.

McConnaughey, T.A., Whelan, J.F., 1997. Calcification generates protons for nutrient and bicarbonate uptake. Earth Sci. Rev. 42 (1–2), 95–117. https://doi.org/10.1016/S0012-8252(96)00036-0.

McConnaughey, T.A., LaBaugh, J.W., Rosenberry, D.O., Striegl, R.G., Reddy, M.M., Schuster, P.F., Carter, V., 1994. Carbon budget for a groundwater-fed lake: calcification supports summer photosynthesis. Limnol. Oceanogr. 39 (6), 1319–1332. https://doi.org/10.4319/lo.1994.39.6.1319.

Megard, R.O., 1968. Planktonic photosynthesis and the environment of calcium carbonate deposition in lakes. SIL Commun., 1953-1996 17 (1), 94. https://doi.org/10.1080/05384680.1969.11903873.

Michard, G., 2002. Chimie des eaux naturelles – Principes de Géochimie des Eaux. Publisud, pp. 1–473.

Millero, F.J., 1979. The thermodynamics of the carbonate system in seawater. Geochim. Cosmochim. Acta 43 (10), 1651–1661. https://doi.org/10.1016/0016-7037(79)90184-4.

Müller, B., Wang, Y., Wehrli, B., 2006. Cycling of calcite in hard water lakes of different trophic states. Limnol. Oceanogr. 51 (4), 1678–1688. https://doi.org/10.4319/lo.2006.51.4.1678.

Müller, B., Meyer, J.S., Gächter, R., 2016. Alkalinity regulation in calcium carbonate-buffered lakes. Limnol. Oceanogr. 61 (1), 341–352. https://doi.org/10.1002/lno.10213.

Obst, M., Wehrli, B., Dittrich, M., 2009. CaCO3 nucleation by cyanobacteria: laboratory evidence for a passive, surface-induced mechanism. Geobiology 7 (3), 324–347. https://doi.org/10.1111/j.1472-4669.2009.00200.x.

Ohlendorf, C., Sturm, M., 2001. Precipitation and dissolution of calcite in a swiss high alpine lake. Arct. Antarct. Alp. Res. 33 (4), 410–417. https://doi.org/10.2307/1552550.

Pacton, M., Ariztegui, D., Wacey, D., Kilburn, M.R., Rollion-Bard, C., Farah, R., Vasconcelos, C., 2012. Going nano: a new step toward understanding the processes governing freshwater ooid formation. Geology 40 (6), 547–550. https://doi.org/10.1130/G32846.1.

Parvathi, A., Zhong, X., Ram, A.S.P., Jacquet, S., 2014. Dynamics of auto- and heterotrophic picoplankton and associated viruses in Lake Geneva. Hydrol. Earth Syst. Sci. 18 (3), 1073–1087. https://doi.org/10.5194/hess-18-1073-2014.

Perga, M.-E., Maberly, S.C., Jenny, J.-P., Alric, B., Pignol, C., Naffrechoux, E., 2016. A century of human-driven changes in the carbon dioxide concentration of lakes. Glob. Biogeochem. Cycles 30 (2), 93–104. https://doi.org/10.1002/2015GB005286.

Perolo, P., Castro, B.F., Escoffier, N., Lambert, T., Bouffard, D., Perga, M.E., 2021. Accounting for surface waves improves gas flux estimation at high wind speed in a large lake. Earth Syst. Dyn. 12 (4), 1169–1189. https://doi.org/10.5194/esd-12-1169-2021.

Plummer, L.N., Busenberg, E., 1982. The solubilities of calcite, aragonite and vaterite in CO2-H2O solutions between 0 and 90°C, and an evaluation of the aqueous model for the system CaCO3-CO2-H2O. Geochim. Cosmochim. Acta 46 (6), 1011–1040. https://doi.org/10.1016/0016-7037(82)90056-4.

Read, J.S., Hamilton, D.P., Jones, I.D., Muraoka, K., Winslow, L.A., Kroiss, R., et al., 2011. Derivation of lake mixing and stratification indices from high-resolution lake buoy data. Environ. Model. Softw. 26 (11), 1325–1336. https://doi.org/10.1016/j.envsoft.2011.05.006.

Read, J.S., Hamilton, D.P., Desai, A.R., Rose, K.C., MacIntyre, S., Lenters, J.D., et al., 2012. Lake-size dependency of wind shear and convection as controls on gas exchange. Geophys. Res. Lett. 39 (9). https://doi.org/10.1029/2012GL051886.

Rimet, F., Anneville, O., Barbet, D., Chardon, C., Crepin, L., Domaizon, I., et al., 2020. The observatory on LAkes (OLA) database: sixty years of environmental data accessible to the public. J. Limnol. 79 (2), 164–178. https://doi.org/10.4081/jlimnol.2020.1944ï.

Sand-Jensen, K., Martinsen, K.T., Jakobsen, A.L., Sø, J.S., Madsen-Østerbye, M., Kjær, J.E., Kristensen, E., Kragh, T., 2021. Large pools and fluxes of carbon, calcium and phosphorus in dense charophyte stands in ponds. Sci. Total Environ. 765. https://doi.org/10.1016/j.scitotenv.2020.142792.

Stabel, H.-H., 1986. Calcite precipitation in Lake Constance: chemical equilibrium, sedimentation, and nucleation by algae. Limnol. Oceanogr. 31 (5), 1081–1094. https://doi.org/10.4319/lo.1986.31.5.1081.

Stets, Edward G., Striegl, R.G., Aiken, G.R., Rosenberry, D.O., Winter, T.C., 2009. Hydrologic support of carbon dioxide flux revealed by whole-lake carbon budgets. J. Geophys. Res. Biogeosci. 114 (1), 1–14. https://doi.org/10.1029/2008JG000783.

Tranvik, L.J., Downing, J.A., Cotner, J.B., Loiselle, S.A., Striegl, R.G., Ballatore, T.J., et al., 2009. Lakes and reservoirs as regulators of carbon cycling and climate. Limnol. Oceanogr. 54 (6 PART 2), 2298–2314. https://doi.org/10.4319/lo.2009.54.6_part_2.2298.

Wanninkhof, R., Knox, M., 1996. Chemical enhancement of CO2 exchange in natural waters. Limnol. Oceanogr. 41 (4), 689–697. https://doi.org/10.4319/lo.1996.41.4.0689.

Wüest, A., Bouffard, D., Guillard, J., Ibelings, B.W., Lavanchy, S., Perga, M.E., Pasche, N., 2021. LéXPLORE: a floating laboratory on Lake Geneva offering unique lake research opportunities. Wiley Interdiscip. Rev. Water 8 (5). https://doi.org/10.1002/wat2.1544.

Zhu, T., Dittrich, M., 2016. Carbonate precipitation through microbial activities in natural environment, and their potential in biotechnology: a review. Front. Bioeng. Biotechnol. https://doi.org/10.3389/fbioe.2016.00004.

Zobrist, J., Schoenenberger, U., Figura, S., Hug, S.J., 2018. Long-term trends in swiss rivers sampled continuously over 39 years reflect changes in geochemical processes and pollution. Environ. Sci. Pollut. Res. 25 (17), 16788–16809. https://doi.org/10.1007/s11356-018-1679-x.